ORTHORECTIFICATION OF BILSAT IMAGERY
USING RIGOROUS AND SIMPLE GEOMETRIC MODELS

A. O. Ok [a] and M. Turker [b]

[a] METU, Graduate School of Natural and Applied Sciences, Geodetic and Geographic Information Techn. Prog. 06531 Ankara, Turkey - oozgun@metu.edu.tr
[b] Hacettepe University, Faculty of Engineering, Department of Geodesy and Photogrammetry, 06800, Beytepe, Ankara, Turkey - mturker@hacettepe.edu.tr

Commission VI, WG VI/4

ABSTRACT:

The orthorectification accuracies of Bilsat Multispectral (XS) imagery using a rigorous and eight simple geometric models are presented. Majority of the selected test area was covered by the existing large scale digital orthophotos, which were used as the source to collect Ground Control Points (GCPs). For the orthorectification process, a DEM generated from stereo ASTER images was used. The developed rigorous model utilizes the well known collinearity condition equations to model the physical reality of the Bilsat sensor. The initial attitude and position information were obtained from the given ephemeris data and the refinement was carried out using an iterative least squares adjustment procedure. The simple geometric models used include the 2D polynomials (1st, 2nd and 3rd order), Rational Functions (1st, 2nd and 3rd order), Projective Transformation (1st order), and Direct Linear Transformation (DLT) (1st order) models. It was found that, using 4 GCPs and 40 Independent Check Points (ICPs), the rigorous model produced RMS errors of 0.75 and 1.14 pixels respectively, for GCPs and ICPs. It was also found that, if a reasonable number of GCPs are used, the rigorous model provides a RMS error of around one pixel for ICPs. Among the simple geometric models used, the 1st order 2D Polynomial model provided the highest RMS error of 3 pixels. On the other hand, the DLT model produced the lowest RMS error of 0.61 and 1.09 pixels for GCPs and ICPs, respectively.

1. INTRODUCTION

BILSAT-1 satellite was successfully launched on September 27, 2003. It is a 129 kg microsatellite in a circular sun-synchronous low Earth orbit, at an altitude of 686 km. Table 1 summarizes the orbital characteristics of the BILSAT-1 satellite. The major satellite payloads consist of 12.6 meter panchromatic and 27.6 meter 4 channel multispectral sensors. Furthermore, a low resolution multispectral (8-band) R&D camera (COBAN) and a real time JPEG2000 image compression DSP card (GEZGIN) both developed by Turkish engineers are accommadated on the satellite (Bradford et. al., 2002). The panchromatic and multispectral sensors have a CCD frame of 2048x2048 pixels and provide 8 bit data (Yuksel et. al., 2004). The satellite also provides stereoscopic images as a result of its three-axis control mode which gives satellite the ability to rotate about any defined axis up to +/- 30 degrees. This property gives opportunity to acquire off-track images which reduces the revisit time of the satellite around 4 days. Technical specifications of the BILSAT-1 sensors are given in Table 2.

BILSAT-1 is also a member of DMC (Disaster Monitoring Constellation) which is an international partnership led by SSTL, comprising a network of five small satellites and ground stations (DMC Constellation, 2005). This constellation enables monitoring and delivery of satellite data concerning disasters occured whereever on Earth and offers daily images at the equator and several imaging opportunities per day at higher altitudes. As a result, the DMC Consortium formed the first-ever microsatellite constellation bringing remarkable Earth observation capabilities both nationally and internationally.

The main objective of this study is to assess the accuracies of the orthorectification of Bilsat Multispectral (XS) imagery using a rigorous geometric model. Then, the accuracies were evaluated for eight simple geometric models. The accuracies were calculated using different numbers and distributions of the GCPs and ICPs. These objectives were met by implementing the model in a selected study area of a size of 52 x 53 km enclosing the city of Ankara.

Parameter	Specification
Orbital path	Circular Sun-synchronous
Orbital period	97.7 min
Altitude	686 km
Inclination	98°
Number of orbits per day	14
Turkey crossing at local time	10:30 am
Revisit time	4 days (XS) 5 days (PAN)
Repeat cycle	52 days (XS) 116 days (PAN)

Table 1. Orbital characteristics of BILSAT-1

Sensor	PAN	XS
Pixel size	12.6 m	27.6 m
Swath width	55x55 km	25x25 km
CCD size	2048x2048	2048x2048
Quantization	8 bit	8 bit
Number of bands	1	4

Table 2. Technical specifications of the BILSAT-1 sensors

2. STUDY AREA AND DATA SETS

2.1 Study Area

The study area is located in central Anatolia. It covers an area of approximately 55 x 55 km and encloses the city of Ankara (Fig. 1). There are also several scattered small towns in the study area. Lakes Mogan and Eymir represented with letter 'B' in Figure 1 are situated in the central part of the study area. There are also several small water bodies randomly distributed in the area. A part of the eastern site (letter 'C' in Figure 1) is rather mountainous. The forested areas are mostly located in the southern part of the city of Ankara and the south western part of the mountainous areas (letter 'D' in Figure 1). The rest of the study area is characterized by the mixture of agricultural areas and open lands (letter 'E' in Figure 1). The elevations range from approximately 700 m for the flat areas to 1900 m for the mountainous areas yielding a total relief around 1200 m. The slopes change sharply in mountainous regions approaching up to 70 degrees.

This area was selected as it contains various land-use and land-cover types such as urban, forest, water, mountainous, agriculture and open lands. The other reason is that both in the city of Ankara and in rural areas, many large roads and paths exist that can be used for selecting the GCPs and ICPs.
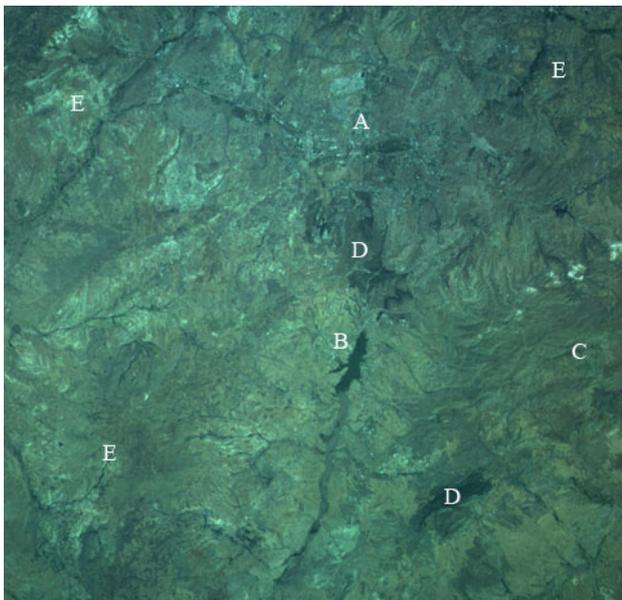

Fig. 1. BILSAT image of the study site. (A) represents the city center of Ankara, (B) represents Lake Mogan, (C) represents the mountainous sites, (D) represents the forestry areas, and (E) represents the agricultural and open lands.

2.2 Data Sets

The BILSAT-1 XS image was acquired on August 03, 2005 (Fig. 1). The image covers an area of approximately 52 x 53 km and completely free from clouds and snow. An imaging survey file, which comprises a number of parameters including the attitude and position data of the satellite during the image acquisition, was also appended to the image data. Because the multispectral image of BILSAT-1 is composed of four separate cameras, each image (three visible and an infrared) has to be transformed to produce a colourful image. The process of the transformation and the parameters calculated for the transformation using least squares adjustment is given and explained in Yuksel et. al. (2004). The transformation of the BILSAT-1 XS bands based on the red channel was performed by the BILSAT team at TUBITAK-BILTEN ground station.

The Ground Control Points (GCPs) were obtained from 1:5000-scale digital orthophotos covering 60% of the study area. The orthophotos were produced in 1999 and referred to the European ED 50 datum and the Transverse Mercator (Gauss – Krueger) projection. The pixel size of the digital orthophotos is 1 m, with an estimated planimetric accuracy of around 20 cm. During the collection of the GCPs, digital orthophotos and the BILSAT image were displayed simultaneously on the screen. As a result, a total of 44 GCPs were collected from the image and the corresponding digital orthophotos. The elevations of the GCPs were obtained from the DEM which was generated using 1:1000-scale vector data. The vector dataset contains the contour lines (drawn with 1 m interval), individual height points, road network, and valley creeks. The accuracy of the vector data is approximately 20 cm both in planimetry and elevation. Consequently, the accuracy of the collected GCPs was estimated to be better than 1 m both in planimetry and elevation.

Because the DEM generated from the vector data covers 60% of the BILSAT-1 image, a different DEM which covers 93% of the image was utilized during the orthorectification process. This DEM was generated from stereo ASTER images using the Orthoengine module of PCI Geomatica image analysis software. The evaluation of the accuracy of the generated DEM was performed based on different parameters including the check points (CPs), slopes and land cover types in a previous study conducted by Ok and Turker (2005). Finally, the accuracy was assessed using 2,171,664 elevation points and the overall accuracy of the DEM was computed to be 10.92 m.

3. SENSOR MODELS FOR ORTHORECTIFICATION

The raw images that are taken from different platforms generally contain several distortions. These distortions can be classified in six main categories and can be summarized as distortions due to platform variations, sensor, instrument and viewing angle errors, atmospheric effects, Earth based distortions and map projections errors (Toutin, 2004). All these distortions must be modelled and corrected by using a specific mathematical model. Several mathematical models can be used for this purpose but the availability of the ephemeris and attitude data directly influences the model type. If the position and the attitude data of the sensor are known during the image acquisition, a rigorous model can be used. Otherwise, a simple geometric model must be used in order to cope with these distortions.

3.1 Rigorous Geometric Model

A rigorous model is a complex model which uses the physical reality of the sensor by integrating the knowledge of the ephemeris and attitude data. A common example of a physical model is the frame camera model, with its usual parameterization (McGlone, 1996):

- Exterior orientation
  - Location: X_L, Y_L, Z_L in a Cartesian object space coordinate system.
  - Orientation: Omega (ω), Phi (φ), Kappa (κ), defined with respect to a Cartesian object space coordinate system, expressed by a 3 by 3 rotation matrix M.

- Interior orientation
  - Focal length (principal distance)
  - Principal point coordinates with respect to fiducial point coordinate system.

- Systematic error corrections
  - Lens distortion
  - Atmospheric refraction

Several models and considerable research have been carried out but the milestone of all the models to derive a rigorous model is the very well known photogrammetric collinearity conditions:

$$x - x_0 = -f \frac{m_{11}(X - X_L) + m_{12}(Y - Y_L) + m_{13}(Z - Z_L)}{m_{31}(X - X_L) + m_{32}(Y - Y_L) + m_{33}(Z - Z_L)} \quad (1)$$

$$y - y_0 = -f \frac{m_{21}(X - X_L) + m_{22}(Y - Y_L) + m_{23}(Z - Z_L)}{m_{31}(X - X_L) + m_{32}(Y - Y_L) + m_{33}(Z - Z_L)} \quad (2)$$

where (x, y) are the image space coordinates of a point, X, Y, Z are the object space coordinates of the point L, X_L, Y_L, Z_L are the object space coordinates of the perspective centre, f is the focal length of the sensor, x_0 and y_0 are the coordinates of the principal point usually known from camera calibration and m_{ij} are the typical elements of a rotation matrix M representing the ω, φ, κ rotations of the image coordinates with respect to the ground coordinates as follows:

$$M = \begin{bmatrix} \cos\varphi\cos\kappa \\ \sin\omega\sin\varphi\cos\kappa + \cos\omega\sin\kappa \\ -\cos\omega\sin\varphi\cos\kappa + \sin\omega\sin\kappa \end{bmatrix}$$

$$\begin{matrix} \cos\varphi\sin\kappa & \sin\omega \\ -\sin\omega\sin\varphi\sin\kappa + \cos\omega\cos\kappa & -\sin\omega\cos\varphi \\ \cos\omega\sin\varphi\sin\kappa + \sin\omega\cos\kappa & \cos\omega\cos\varphi \end{matrix}_{3x3} \quad (3)$$

In the case of BILSAT imagery, the images are taken as the snapshots using a 2048x2048 pixel frame CCD array. Because a frame sensor acquires the whole image at an instant of time, the exterior orientation parameters of a frame camera images are fixed. Therefore, the regular collinearity conditions and the rotation matrix can be used to relate the image space and the object space without any modification. The level of the detail to be modelled in rigorous models does not always reflect a substantial increase in terms of required level of accuracy. For example, lens distortion is often neglected for modern mapping cameras since its magnitude is usually not more than a few micrometers, while atmospheric refraction is usually neglected for low-altitude imagery (McGlone, 1996). Therefore, in this study, both parameters are neglected. In addition, because the calibration information concerning the XS sensor was not available, the difference between the principal point coordinates with respect to fiducial point coordinate system was assumed to be zero and the focal length was used to be 180 mm without performing any correction. On the other hand, these assumptions also give opportunity to determine the level of orthorectification accuracy of BILSAT-1 XS without taking into account these corrections.

In this study, the exterior orientation parameters, which are embedded in the collinearity equations, were estimated using different number of GCP sets through iterative least squares estimation procedure. Each GCP gives rise to a measurement vector which consists of five observations, two image space coordinates of the raw image and three object space coordinates on the ground. The six elements of the exterior orientation parameters (X_L, Y_L, Z_L, ω, φ and κ) form the parameter vector as:

$$\beta = \begin{bmatrix} X_L & Y_L & Z_L & \omega & \varphi & \kappa \end{bmatrix}^T \quad (4)$$

In the estimation procedure, the initial values for the parameters are required. The initial object space coordinates of the perspective centre is obtained from the given ephemeris data. Therefore, the initial parameter vector turns into the form:

$$\beta^0 = \begin{bmatrix} X_L^0 & Y_L^0 & Z_L^0 & 0 & 0 & 0 \end{bmatrix}^T \quad (5)$$

Because the collinearity equations are non-linear, they have to be linearized prior to the formulation of the normal equations of the least squares adjustment to be solved by using successive iterations. To do that, the X matrix which is the matrix of the observation equations (also called coefficient matrix) is formed by taking the partial derivatives of equations (1, 2) with respect to the elements of β:

$$X = \begin{bmatrix} \frac{\partial F_1}{\partial X_L} & \frac{\partial F_1}{\partial Y_L} & \frac{\partial F_1}{\partial Z_L} & \frac{\partial F_1}{\partial \omega} & \frac{\partial F_1}{\partial \varphi} & \frac{\partial F_1}{\partial \kappa} \\ \frac{\partial F_2}{\partial X_L} & \frac{\partial F_2}{\partial Y_L} & \frac{\partial F_2}{\partial Z_L} & \frac{\partial F_2}{\partial \omega} & \frac{\partial F_2}{\partial \varphi} & \frac{\partial F_2}{\partial \kappa} \\ \cdot & & \cdot & & & \cdot \\ \cdot & & \cdot & & & \cdot \\ \frac{\partial F_{n-1}}{\partial X_L} & \frac{\partial F_{n-1}}{\partial Y_L} & \frac{\partial F_{n-1}}{\partial Z_L} & \frac{\partial F_{n-1}}{\partial \omega} & \frac{\partial F_{n-1}}{\partial \varphi} & \frac{\partial F_{n-1}}{\partial \kappa} \\ \frac{\partial F_n}{\partial X_L} & \frac{\partial F_n}{\partial Y_L} & \frac{\partial F_n}{\partial Z_L} & \frac{\partial F_n}{\partial \omega} & \frac{\partial F_n}{\partial \varphi} & \frac{\partial F_n}{\partial \kappa} \end{bmatrix}_{nx6} \quad (6)$$

The normal equations are formed from these observation equations. During the estimations, the increments for the six unknowns are computed and used to update the approximations for the parameters of the subsequent iterations. The estimation continues until the differences between the parameters become

negligible. The least squares solution to this system is formed as:

$$\Delta\beta = (X^T\ W\ X)^{-1}\ X^T\ W\ \Delta Y \qquad (7)$$

where, a priori weight matrix W taken as an identity matrix in this case.

3.2 Simple Geometric Models

A simple geometric model usually involves mathematical models, which are easier to understand and do not require the knowledge of image sensor physics (Toutin, 2004). These systems neither use nor require information related to the sensor, platform, the Earth, and do not reflect the geometry of the distortions. In this respect, simple geometric models require simple mathematical models to relate the image space and object space.

Different mathematical models involve different number of unknown parameters which must be solved with the help of the GCPs collected throughout the image. The adjustment of these parameters can be performed by using the least squares adjustment process which is mentioned in the previous part. Once the parameters are determined, the correct positions of each pixel in the image can be estimated by these models.

Until now, a number of different simple geometric models with different orders are introduced:

- 2D Polynomial Models
- Rational Functions
- Projective Transformation
- Direct Linear Transformation

3.2.1 2D Polynomial Models

In this method, the relation between the image space and the object space is performed by using only the planimetric coordinates of the GCPs. The general mathematical formulation of a 2D polynomial function can be expressed as (Toutin, 2004):

$$P_{2D}(x,y) = \sum_{i=0}^{m}\sum_{j=0}^{n} a_{ij} X^i Y^j \qquad (8)$$

where, X and Y are the planimetric coordinates of the GCPs, i and j are the increment values, m and n determine the order of the polynomial model, generally between one and five, and a_{ij} are the polynomial coefficients to be determined by the least squares approach. Because, 2D Polynomial models do not take into account the elevations of the GCPs these models can be efficiently used when the image area is relatively flat, namely where the image is not influenced by the topographic effects. Furthermore, in order to achieve a good accuracy, GCPs have to be accurate, numerous and evenly distributed across the image.

3.2.2 Rational Functions

Rational Functions perform transformations between the image and the object spaces through a ratio of 3D polynomials. The general form of the rational functions can be written as (Toutin, 2004):

$$R_{3D}(x,y) = \frac{\sum_{i=0}^{m}\sum_{j=0}^{n}\sum_{p=0}^{p} a_{ijk} X^i Y^j Z^k}{\sum_{i=0}^{m}\sum_{j=0}^{n}\sum_{p=0}^{p} b_{ijk} X^i Y^j Z^k} \qquad (9)$$

where a_{ijk} are the polynomial coefficients that are called rational functions. One important difference of the rational functions is that both the image coordinates (x,y) and the object coordinates (X, Y, Z) are normalized to fit the range from -1 to +1 to minimize the errors during the computations and improve the numerical stability of the equations.

In this study, the rational functions coefficients are estimated from the available GCPs, which is also called the terrain dependent method. One major disadvantage is that the increase of the Rational function coefficients (RFCs) also increases the possibility of the correlation between the RFCs and can make the least squares estimation instable.

3.2.3 Projective Transformation

The projective transformation describes the relationship between the two planes (Novak, 1992). It is the basic fractional model which can relate the image space and the object space. It integrates only the planimetric coordinates as the 2D polynomial model. The projective transformation is also called eight parameter transformation because the total of unknowns of the model are eight:

$$x = \frac{a_1 X + a_2 Y + a_3}{c_1 X + c_2 Y + 1} \qquad y = \frac{b_1 X + b_2 Y + b_3}{c_1 X + c_2 Y + 1} \qquad (10)$$

where, a_1, a_2, a_3, b_1, b_2, b_3, c_1, and c_2 are the eight unknown parameters of the functions.

3.2.4 Direct Linear Transformation (DLT)

The DLT models the transformation between the image pixel coordinate system and the object space coordinate system as a linear function (Mikhail et. al., 2001). It has been widely used in close range photogrammetry and the model is often used to derive the approximate initial values of unknown parameters for the collinearity equations. DLT has three additional unknowns when compared to the Projective Transformation:

$$x = \frac{a_1 X + a_2 Y + a_3 Z + a_4}{c_1 X + c_2 Y + c_3 Z + 1} \qquad y = \frac{b_1 X + b_2 Y + b_3 Z + b_4}{c_1 X + c_2 Y + c_3 Z + 1}$$

where, a_1, a_2, a_3, a_4, b_1, b_2, b_3, b_4, c_1, c_2, and c_3 are the linear orientation parameters between two dimensional image space and the three dimensional object space.

4. THE RESULTS

The models used for the orthorectification process include (1) Rigorous model, (2-4) 2D polynomials (first to third degree), (5-7) Rational Functions (first to third degree), (8) Projective Transformation (1st degree), and (9) Direct Linear Transformation (DLT) (1st degree) models. All mathematical models were developed using Matlab 6.5.0 and implemented using macros.

4.1 The Results of the Rigorous Geometric Model

Table 3 summarizes the performance of the rigorous model under different evenly distributed GCP and ICP combinations. All these errors are given and evaluated in the image space.

When 4 GCPs are used, the rigorous model produced an overall RMSE of 0.75 pixels for GCPs and 1.14 pixels for ICPs. When the GCP number is increased, the GCP RMSE is stabilized around 1 pixel. However, the ICP RMSE reached the lowest RMSE when 28 GCPs are used and had an RMSE of 1 pixel. When all available points are used as GCPs, the RMSE was computed as 0.99 pixels. Therefore, it can be stated that the increase in the number of the GCPs did not improve the accuracy of overall rigorous geometric model significantly.

The error vector diagram of the rigorous model obtained using 44 GCPs demonstrates that the RMSE of the points are completely random (Figure 2). However, it is clear that the points that are located sparsely had more deteriorated RMSE values than the ones that are closer to each other. Therefore, it is possible to expect worse RMSE values for the isolated points.

In addition to the assessments of the evenly distributed GCPs, a different analysis which emphasizes the performance of the rigorous model under different unevenly distributed GCPs was also performed. In this analysis, initially, three different groups each consisting of 4 unevenly distributed GCPs were selected. The rest of the points in these groups were considered as ICPs. Later, the analysis was repeated using three different groups each containing unevenly distributed 12 GCPs. Similarly, the remaining 32 points in these groups were labelled ICPs. Initializing this analysis with a total of two different groups each containing 3 different combinations gave a thought of attainable accuracies from the rigorous model when unevenly distributed GCPs are used. The results are presented in Table 4.

As can be seen in Table 4, although the GCPs were selected only from a small part of the image, very good GCP RMSE values were obtained. But, if we compare the ICP results with the evenly distributed results, a clear deterioration in the ICP RMSE values is observed. However, especially for the last three sets, the results seem to be quite good because these results were obtained in a condition where the GCPs are localized and not evenly distributed. As a result, using 12 unevenly distributed GCPs, the rigorous model would produce a total ICP accuracy of around 3 pixels at most where the GCPs are not available for the most of the image.

GCPs / ICPs	GCP RMS Error (pixel)			ICP RMS Error (pixel)		
	X	Y	XY	X	Y	XY
4 / 40	0.65	0.37	0.75	0.80	0.82	1.14
8 / 36	0.54	0.36	0.65	0.83	0.74	1.11
12 / 32	0.71	0.44	0.84	0.81	0.74	1.10
16 / 28	0.74	0.41	0.85	0.79	0.77	1.10
20 / 24	0.69	0.48	0.84	0.83	0.79	1.15
24 / 20	0.80	0.55	0.97	0.76	0.78	1.09
28 / 16	0.78	0.64	1.01	0.75	0.66	1.00
32 / 12	0.74	0.65	0.98	0.84	0.64	1.06
44 / -	0.75	0.64	0.99	-	-	-

Table 3. The results of the rigorous model for different number of evenly distributed GCPs.
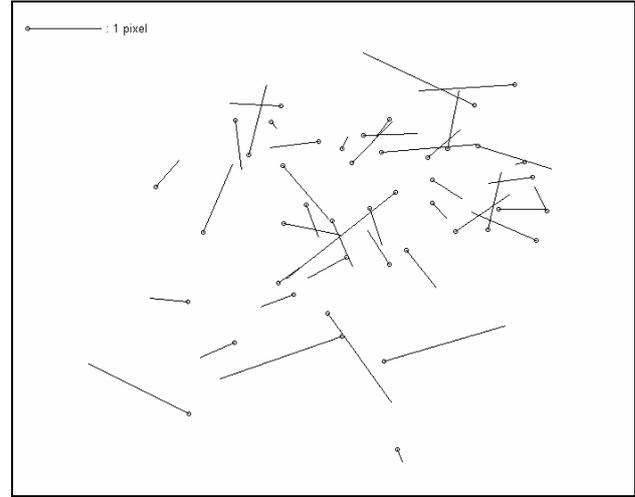

Fig. 2. Error vectors for the rigorous model using 44 GCPs.

Combinations		GCP Total RMSE	ICP Total RMSE
4 GCPs / 40 ICPs	Group 1	0.33	4.05
	Group 2	0.04	6.38
	Group 3	0.19	2.48
12 GCPs / 32 ICPs	Group 1	0.62	1.97
	Group 2	0.71	2.78
	Group 3	0.78	1.67

Table 4. The results of the rigorous model for different number of unevenly distributed GCPs.

4.2 The Results of the Simple Geometric Models

The results of the orthorectification of simple geometric models are given in Table 5. Among the simple geometric models used, the model 1st order 2D Polynomial provided the highest RMS error of 3 pixels. In addition, models 2nd and 3rd order 2D Polynomials and Projective Transformation also did not produce satisfactory ICP results even higher numbers of GCPs were used.

The DLT model produced the lowest ICP RMS error of 1.11 pixels when 20 GCPs were used. The model also produced very good GCP and ICP RMSE values when 12 GCPs were used. Therefore, the DLT model seems to be the best model to orthorectify BILSAT images among the simple geometric models. The 1st order Rational Function produced similar results to the model DLT when 20 GCPs were used. The 2nd order Rational Function also produced similar results when 32 GCPs were used. Even though the model 3rd order Rational Function produced the best GCP accuracies, it is completely useless due to its excessive number of GCP requirement. One other disadvantage of the 2nd and 3rd order Rational Functions is the correlations necessary between the parameters inside the models. Therefore, these models require the regularization to the normal equations in the least squares adjustment process. Only after the regularization process, the matrix $X^T X$ in normal equations will became invertible. In this study, the Tikhonov regularization was used to solve this problem in the models 2nd and 3rd order Rational Functions. However, these models still seem to be instable due to the implementation of the regularization process.

Model	Order	GCPs / ICPs	GCP RMS Error (pixel)			ICP RMS Error (pixel)		
			X	Y	XY	X	Y	XY
2D Polynomial	1	4 / 40	1.25	3.52	3.74	6.18	2.62	6.71
		20 / 24	2.49	2.57	3.58	2.25	1.52	2.72
		44 / 0	2.22	2.01	3.00	-	-	-
	2	7 / 37	0.21	0.21	0.29	1.10	0.79	1.35
		20 / 24	0.74	0.38	0.83	1.04	0.88	1.36
		44 / 0	0.87	0.66	1.09	-	-	-
	3	11 / 33	0.52	0.23	0.57	1.14	2.30	2.57
		20 / 24	0.61	0.36	0.71	0.98	0.91	1.34
		44 / 0	0.77	0.65	1.00	-	-	-
Rational Functions	1	8 / 36	0.17	0.05	0.18	0.73	2.67	2.77
		20 / 24	0.39	0.40	0.56	0.81	0.90	1.21
		44 / 0	0.60	0.65	0.88	-	-	-
	2	20 / 24	0.21	0.20	0.29	1.31	1.27	1.82
		32 / 12	0.49	0.44	0.95	0.54	1.03	1.16
		44 / 0	0.48	0.58	0.76	-	-	-
	3	40 / 4	0.30	0.28	0.41	0.92	1.51	1.77
		44 / 0	0.44	0.46	0.63	-	-	-
Projective Transformation	1	9 / 35	1.03	2.13	2.37	1.42	1.63	2.16
		20 / 24	0.81	0.87	1.18	1.14	0.87	1.43
		44 / 0	0.94	0.82	1.25	-	-	-
DLT	1	12 / 32	0.36	0.50	0.61	0.79	0.75	1.09
		20 / 24	0.46	0.47	0.66	0.74	0.82	1.11
		44 / 0	0.60	0.66	0.89	-	-	-

Table 5. The results of the simple geometric models for different number of evenly distributed GCPs.

5. CONCLUSION

In this study, the orthorectification accuracies of Bilsat Multispectral (XS) imagery using a rigorous and eight simple geometric models are presented. Based on the results obtained, the orthorectification accuracy of around 1 pixel can be easily achieved from the developed rigorous model using the uniformly distributed 4 GCPs. In addition, if a reasonable number of unevenly distributed GCPs are available, the rigorous model may produce accuracies similar to the most of the simple geometric model accuracies that are generated using evenly distributed GCP sets.

In terms of simple geometric models, The DLT model produced the lowest ICP RMS error for all GCP and ICP combinations. Therefore, the DLT model seems to be the best simple geometric model to orthorectify BILSAT images.

REFERENCES

Bradford, A., Gomes, L. M., Sweeting, M., Yuksel, G., Ozkaptan C., Orlu, U., 2002. BILSAT-1: A Low Cost, Agile, Earth Observation Microsatellite for Turkey. 53rd International Astronautical Congress, Houston, Texas, USA.

DMC Constellation, 2005. DMC International Imaging Ltd. http://www.dmcii.com/products_constellation.htm (accessed 14 Dec. 2005).

McGlone, C., 1996. Sensor modeling in image registration. Digital Photogrammetry. American Society for Photogrammetry and Remote Sensing, Bethesda, Maryland. pages: 115–123.

Mikhail, E. M., Bethel, J. S., and McGlone, J. C., 2001. Introduction to Modern Photogrammetry.

Neumaier, A., 1998. Solving Ill-Conditioned and Singular Linear Systems: A Tutorial on Regularization, SIAM Review, Vol. 40, No. 3, pp. 636-666.

Novak, K., 1992. Rectification of Digital Imagery, Photogrammetric Engineering and Remote Sensing, Vol. 58, No. 3, pp. 339-344.

Ok, A. O., Turker, M., 2005. DEM Generation and Accuracy Assessment from Stereo ASTER Imagery. Proceedings of the 2nd International Conference on Recent Advances in Space Technologies, pp. 523-528, Istanbul, Turkey.

Toutin, T., 2004. Review Article: Geometric Processing of Remote Sensing Images: Models, Algorithms and Methods, International Journal of Remote Sensing, Vol. 25, No. 10, pp. 1893-1924.

Yuksel, G., Belce, O., Urhan, H., Gomes, L., Bradford, A., Bean, N., Curiel, A. S., 2004. BILSAT-1: First Year in Orbit-Operations and Lessons Learned. The 18th Annual AIAA/USU Conference on Small Satellites, Logan, Utah, USA.